PNAS RESEARCH ARTICLE | PHARMACOLOGY

An analgesic peptide H-20 attenuates chronic pain via the PD-1 pathway with few adverse effects

Long Zhao[a,1], Hao Luo[b,1], Yu Ma[c], Shengze Zhu[a], Yongjiang Wu[a], Muxing Lu[a], Xiaojun Yao[d], Xin Liu[e], and Gang Chen (陈罡)[a,c,f,2]

Edited by Robert Lefkowitz, Howard Hughes Medical Institute, Durham, NC; received March 8, 2022; accepted June 17, 2022

The lack of effective and safe analgesics for chronic pain management has been a health problem associated with people's livelihoods for many years. Analgesic peptides have recently shown significant therapeutic potential, as they are devoid of opioid-related adverse effects. Programmed cell death protein 1 (PD-1) is widely expressed in neurons. Activation of PD-1 by PD-L1 modulates neuronal excitability and evokes significant analgesic effects, making it a promising target for pain treatment. However, the research and development of small molecule analgesic peptides targeting PD-1 have not been reported. Here, we screened the peptide H-20 using high-throughput screening. The in vitro data demonstrated that H-20 binds to PD-1 with micromolar affinity, evokes Src homology 2 domain–containing tyrosine phosphatase 1 (SHP-1) phosphorylation, and diminishes nociceptive signals in dorsal root ganglion (DRG) neurons. Preemptive treatment with H-20 effectively attenuates perceived pain in naïve WT mice. Spinal H-20 administration displayed effective and longer-lasting analgesia in multiple preclinical pain models with a reduction in or absence of tolerance, abuse liability, constipation, itch, and motor coordination impairment. In summary, our findings reveal that H-20 is a promising candidate drug that ameliorates chronic pain in the clinic.

chronic pain | programmed cell death protein 1 | analgesic | Src homology 2 domain–containing tyrosine phosphatase 1 | dorsal root ganglion

Significance

Recently, lots of studies have demonstrated that programmed cell death protein 1 (PD-1) participates in the modulation of neuronal excitability, synaptic transmission, and synaptic plasticity in neurons. It is regarded as an alternative target to address the opioid crisis. However, no related ligands targeting PD-1 with analgesic potential have been reported except PD-L1. In this study, we screened an analgesic peptide H-20, which significantly inhibits acute pain and chronic pain via the PD-1 pathway with few adverse effects in multiple preclinical pain models. This finding will provide ideas for analgesic drug research and development.

Chronic pain is a common refractory disease with an ∼30% prevalence rate among the world's population. The management of chronic pain is a major health problem clinically that causes serious social and economic burdens. There is a high demand for analgesic drugs in the clinic, but their development is lagging. New discoveries regarding the pathogenic mechanisms and means of prevention for chronic pain are significant breakthroughs in the therapeutic bottlenecks. Current-generation analgesics for the treatment of chronic pain rely primarily on antiepileptic drugs, antidepressants, opioid analgesics, capsaicin, and nonsteroidal antiinflammatory drugs (1). However, reduced analgesic effects and increased tolerance, dependence, respiratory depression, gastrointestinal reactions, and hypersensitivity render these drugs suboptimal for long-term administration (2, 3). Therefore, safer and more effective treatments for chronic pain are necessary. Peptides are a rich source of lead compounds during drug development (4–6). Recent clinical and preclinical studies have confirmed that analgesic peptides exert beneficial effects with fewer accompanying side effects (7–9).

Programmed cell death protein 1 (PD-1) is a type I transmembrane glycoprotein that is encoded by the *PDCD1* gene and 288 amino acids in length (50 to 55 kDa). It is divided into three regions: a single lgV-like N-terminal domain, a transmembrane domain, and a cytoplasmic tail. PD-1 is widely expressed on cytotoxic T cells, B cells, natural killer cells, macrophages, microglia, regulatory T cells, and neurons (10–12). For decades, substantial research has found that PD-1 is a crucial negative regulator associated with various biological effects and diseases, including tumor immunotherapy, brain tumors, stroke, Alzheimer's disease, cognitive deficits, and multiple sclerosis (13, 14). To the best of our knowledge, PD-1 signaling modulates neuronal excitability, synaptic transmission, and synaptic plasticity in neurons and has drawn more attention from medicinal chemists (10). Its neuronal signaling regulates pain by activating Src homology 2 domain–containing protein tyrosine phosphatase 1 (SHP-1), modulating sodium/potassium channels (11), dephosphorylating transient receptor potential subtype V1 (TRPV1) (15), and regulating GABAergic neurotransmission (12). *Pd1* knockout ($Pd1^{-/-}$) mice are more sensitive to pain than wild-type (WT) mice, indicating that PD-1 plays a prominent role in pain modulation (11). In addition, the activation of PD-1 signaling by PD-L1 is involved in the regulation of μ-opioid receptor signals on nociceptive neurons to enhance morphine-induced analgesia and improve opioid-related adverse effects (16). Thus, targeting PD-1 with small molecule peptides provides an alternative therapeutic approach for treating chronic pain.

Author contributions: L.Z. and G.C. designed research; L.Z., H.L., Y.M., S.Z., Y.W., M.L., X.Y., and X.L. performed research; L.Z. and G.C. wrote the paper; X.Y. did the binding mode prediction; and X.L. completed the MST experiment.

The authors declare no competing interest.

This article is a PNAS Direct Submission.

[1]L.Z. and H.L. contributed equally to this study.

[2]To whom correspondence may be addressed. Email: chengang6626@ntu.edu.cn.

This article contains supporting information online at http://www.pnas.org/lookup/suppl/doi:10.1073/pnas.2204114119/-/DCSupplemental.

Published July 25, 2022.

Results

Screening of PD-1–Targeted Peptides. Given our improved understanding of the role of PD-1 in neural pathways of pain modulation (10), we constructed a peptide database for PD-1 peptide molecular docking with predicted constraints to identify potential ligands. The molecular docking analysis results provided 22 peptides that target PD-1 with promising docking scores (*SI Appendix*, Table 1). Peptides with amber scores in the [−95, −80] interval were synthesized. Screening of the promising PD-1–targeted peptide was performed again using a carrageenan-induced inflammatory pain model. According to the results of the preexperiment, the inflammatory pain could be alleviated to varying degrees by most of these peptides (intrathecal [i.t.], 20 nmol), including H-4, H-11, H-18, H-19, H-20, H-21, and H-22 (*SI Appendix*, Fig. 1). H-20 (Fig. 1*A*) agreed with our expectations and was selected to further investigate.

Binding of H-20 to PD-1. Further analysis of the interactions between PD-1 and the promising peptide H-20 was conducted using molecular dynamics simulations. The docking score of H-20 was −8.767 kcal/mol (*SI Appendix*, Table 2). The binding mode of PD-1 with H-20 is shown in Fig. 1*B*. According to these results, the important residues in the binding pocket involved in H-20 binding included Val^{64}, Tyr^{68}, Gln^{75}, Thr^{76}, Lys^{78}, Asp^{85}, Ile^{126}, Leu^{128}, Ala^{132}, Ile^{134}, and Glu^{136}. The predicted binding energies of H-20 with PD-1 were calculated via the molecular mechanics/generalized Born surface area (MM/GBSA) methodology. The calculation result was −42.61 kcal/mol, suggesting that H-20 has favorable and stable interactions with PD-1 (*SI Appendix*, Table 2). Microscale thermography (MST) is a new method to verify ligand–protein binding (17–19). Here, we performed a MST assay to further confirm the binding of H-20 with PD-1. The dissociation constant (K_D) value of H-20 to mPD-1 was 57 μM (*SI Appendix*, Fig. 2*A*), indicating that H-20 displayed appreciable binding affinity to PD-1. The K_D value of the positive control mPD-L1 to mPD-1 was 0.78 μM (*SI Appendix*, Fig. 2*B*), which was similar to a previous report (20).

Evaluation of H-20 Stability. As shown in *SI Appendix*, Table 2, the degradation $t_{1/2}$ of H-20 in mouse brain homogenate was 100 min, suggesting long-lasting analgesic potential, which was consistent with the in vivo results.

H-20 Induced SHP-1 Phosphorylation via PD-1. In this study, immunohistochemical methods were used to confirm whether H-20 binds to PD-1 and activates SHP-1 in vivo after i.t. injection. In line with prior work (11), PD-1 is expressed in the membrane surface of dorsal root ganglion (DRG) neurons (Fig. 1*C*). After i.t. injection of HA-H20 (YPYDVPDYAISYGGADYK) into naïve mice, the immunohistochemical results showed that H-20 bound to PD-1 in accordance with the docking and MST results (Fig. 1*D* and *SI Appendix*, Fig. 3). As expected, H-20 induced SHP-1 phosphorylation in DRG neurons (Fig. 1 *E* and *F*). From immunohistochemistry, it is not hard to draw a conclusion that H-20 is similar to PD-L1 and has an analgesic potential.

H-20 Inhibits Capsaicin-Induced $[Ca^{2+}]_i$ Increase and Acute Pain. TRPV1, which responds to nociceptive stimuli such as elevated temperature, reduced pH, vanilloids, and other pain-inducing substances, is an important ion channel associated with peripheral sensitization to pain (15, 21–23). The activation of TRPV1 with capsaicin markedly evoked the influx of extracellular calcium. The results suggested that H-20 suppress TRPV1-mediated $[Ca^{2+}]_i$ response via the PD-1 pathway (Fig. 1*G*). Interestingly, knocking out the *Pd1* gene also attenuates the activation of TRPV1 in cultured DRG neurons, indicating the essential role of PD-1 in the nociception of pain signals (Fig. 1*G*). In addition, H-20 (30 nmol) significantly inhibited capsaicin-induced spontaneous pain behaviors (*SI Appendix*, Fig. 4*A*). Those finding suggested that the pain-modulating pathways of PD-1 are associated with TRPV1 and are consistent with a previous study (15).

H-20 Modulates Basal Pain Thresholds via PD-1. In the present study, we examined whether compound H-20 improved the pain threshold in naïve mice. The pain-related behaviors of naïve mice were measured by the von Frey test. As shown in Fig. 1*H*, preemptive i.t. injection of H-20 (30 nmol) significantly increased the basal mechanical threshold in naïve WT mice (onset of 30 min, duration of at least 150 min), but evidently had no effect on naïve *Pd1* knockout mice ($P > 0.05$). Similar effects were obtained following intravenous (i.v.) administration of H-20 (12 mg/kg) in naïve WT mice (*SI Appendix*, Fig. 4*B*). In addition, i.t. injection of H-20 (30 nmol) was equally capable of raising the thermal pain threshold of the naïve WT mice in the tail flick and hot plate tests (*SI Appendix*, Fig. 4 *C* and *D*).

H-20 Modulates DRG Neuronal Excitability via PD-1. In addition, the effects of H-20 on neuronal excitability in dissociated small-diameter DRG neurons were evaluated using patch-clamp recordings. The data showed that pretreatment with H-20 (300 μM) evoked hyperpolarization of the resting membrane potential (RMP) (Fig. 1 *I* and *J*), significantly attenuated the action potential (AP) induced by current injection, and further increased the rheobase (Fig. 1 *K* and *L*). These effects of H-20 on the RMP and AP were abrogated in $Pd1^{-/-}$ mice. The electrophysiological results indicated that H-20 suppresses neuronal excitability in DRGs via PD-1.

Spinal H-20 Produces Analgesia in a Formalin-Induced Spontaneous Pain Model. In the formalin model, intraplantar injection of 5% formalin evoked a biphasic pain response. As shown in Fig. 2*A* and *SI Appendix*, Fig. 4*E*, i.t. injection of H-20 (1, 10, and 30 nmol) and PD-L1 (10, 40, and 100 pmol) caused mild inhibition of first phase nociceptive response ($P < 0.05$) and dose-dependent inhibition of second phase spontaneous pain behaviors. The reference effective dose 50% of maximum response (ED_{50}) values of PD-L1 and H-20 were 0.004 (0.002, 0.01) nmol and 0.63 (0.35, 1.16) nmol, respectively, for the second phase (*SI Appendix*, Table 3). The spinal analgesic effect of compound H-20 (30 nmol) was comparable to that of PD-L1 (0.1 nmol) or morphine (2 nmol) in both pain phases (*SI Appendix*, Fig. 4*F*). The data in *SI Appendix*, Fig. 4*G* show i.t. coadministration of 10 nmol SHP-1 inhibitor sodium stibogluconate (SGG) clearly attenuated the spinal antinociception of H-20 (30 nmol) in the second phase of pain. Notably, the antinociception of H-20 could not be attenuated by naloxone (coinjection, 5 nmol, *SI Appendix*, Fig. 4*G*), suggesting that the spinal analgesia of H-20 is not mediated by the opioid system. In addition, the spinal antinociception of H-20 (30 nmol) was also abolished in $Pd1^{-/-}$ mice in the second phases of pain (Fig. 2*B*).

Spinal H-20 Reduces the Visceral Pain-Related Behaviors in Mice. In the writhing test, apparent dose-dependent inhibition of writhing behaviors was observed after i.t. injection of H-20

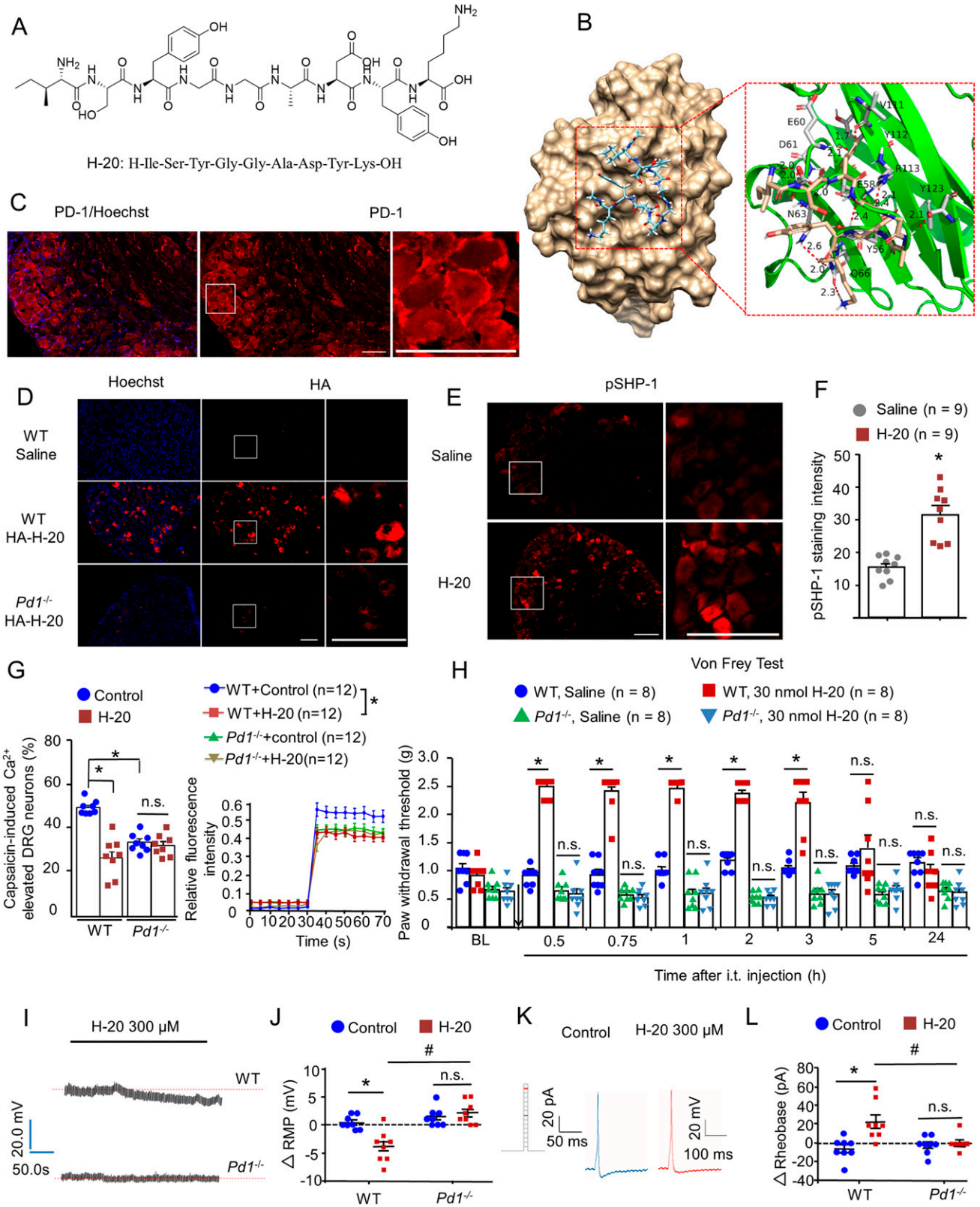

Fig. 1. A peptide ligand of PD-1. (*A*) Chemical structure of H-20. (*B*) Binding mode of H-20 with PD-1 (PDB ID: 4ZQK). (*C*) Expression of PD-1 on DRGs. (Scale, 50 μm.) (*D*) Intrathecal HA–H-20 (30 nmol, 1 h), the in vivo binding of HA–H-20 with PD-1 on DRGs. (Scale, 50 μm.) Four mice per group. (*E* and *F*) Intrathecal H-20 (30 nmol, 1 h) increased SHP-1 phosphorylation in naïve WT mice. (*E*) pSHP-1 immunostaining in DRGs. (Scale bar, 50 μm.) (*F*) Immunofluorescence intensity of pSHP-1 in DRGs. Four mice per group, nine images per group. **P* < 0.05, versus saline group. Student's test. (*G*) Pretreatment with H-20 (300 μM) attenuates capsaicin-induced increase in $[Ca^{2+}]_i$ in cultured DRGs via PD-1. (*Left*) The proportion of neurons responsive to capsaicin. Mean ± SEM **P* < 0.05, versus WT control group. Eight independent experiments for per group. Two-way ANOVA. (*Right*) The typical traces of calcium responses. Twelve neurons per group. **P* < 0.05, versus WT control group. Two separate three-way repeated measures (RMs) ANOVA (0 to 30 and 35 to 70 min). (*H*) H-20 modulates basal mechanical pain thresholds via PD-1. Mean ± SEM **P* < 0.05, versus saline group. Eight mice per group. Three-way RM ANOVA. (*I*–*L*) H-20 modulates neuronal excitability via PD-1. Mean ± SEM eight neurons per group. **P* < 0.05, versus WT + control group. $^{\#}P$ < 0.05, versus WT + H-20 group. n.s., no significance. Two-way ANOVA. (*I* and *J*) H-20 alters hyperpolarization of the RMP in WT mice, but not in $Pd1^{-/-}$ mice. (*K* and *L*) H-20 increases the rheobase in cultured DRGs in WT mice, but not in $Pd1^{-/-}$ mice.

with an ED_{50} value of 3.38 (1.64, 6.92) nmol in WT mice (Fig. 2*C*). The inhibition rate of writhing behaviors of H-20 (30 nmol) significantly decreased from 82 to 29% or 44%, respectively, after knocking out the *Pd1* gene (Fig. 2*D*) or blocking the downstream signaling of PD-1 with SSG (*SI Appendix*, Fig. 4*H*).

Spinal H-20 Produces Analgesia in Inflammatory Pain. Intraplantar injection of λ-carrageenan (1%, Sigma, C1013) into the left hind paw of mice evokes acute inflammatory pain with significantly reduced mechanical allodynia after 1 d. As illustrated in Fig. 2*E*, i.t. injection of H-20 (30 nmol) significantly alleviated carrageenan-induced mechanical allodynia (onset of 30 min, duration of 150 min). The i.v. results confirmed the effectiveness of H-20 after systemic administration for inflammatory pain without an apparent dose dependence (*SI Appendix*, Fig. 4*I*). Administration of complete Freund's adjuvant (CFA) (Sigma, F5881) evoked persistent inflammatory pain with hypersensitivity and paw edema responses that persisted for 2 wk (24). Similar to the carrageenan-induced inflammatory pain test, i.t. H-20 (30 nmol) induced a significant reversal of mechanical allodynia, as shown in Fig. 2*F* and *SI Appendix*, Fig. 4*J* (onset of 30 min, duration of at least 150 min). No significant difference in the analgesic effects of i.t. injection of H-20 (30 nmol) between male and female mice was observed in the CFA-induced inflammatory pain model (*SI Appendix*, Fig. 4*K*).

Spinal H-20 Produces Analgesia in Neuropathic Pain. In recent years, peripheral neuropathic pain caused by anticancer drugs has caused a vast number of chemotherapy patients to suffer and is considered to be a major health care burden. Paclitaxel (PTX), a cancer chemotherapy drug, could induce the dose-limiting adverse effect of neuropathic pain. In this study, a chemotherapy-induced peripheral neuropathy (CIPN) model was established by intermittent intraperitoneal (i.p.) administration of PTX (2 mg/kg) on days 1, 3, 5, and 7. After completing the PTX injection series, CIPN symptoms were observed in the test mice. Mechanical allodynia was assessed by the von Frey method. As shown in Fig. 2*G*, compared to the saline group, H-20 (onset of 30 min, duration of at least 150 min) inhibited PTX-induced nociceptive behaviors, which displayed a potent and long antiallodynic effect on paclitaxel-induced neuropathic pain at the spinal level. Chronic constriction of the sciatic nerve (chronic constriction injury [CCI]) robustly decreased the mechanical threshold of the mice after 7 d of surgery and was sustained for more than 7 wk. Similar to the CIPN model, i.t. H-20 (30 nmol) apparently increased the paw withdrawal threshold (onset of 30 min, duration of at least 150 min) in the CCI neuropathic model (Fig. 2*H*).

H-20 Inhibits Neuronal Hyperexcitability after Nerve Injury. In the current study, spared nerve injury (SNI)-induced neuronal hyperexcitability in small nociceptive DRG neurons was measured using patch-clamp recordings. As expected, SNI-induced DRG nociceptive neurons showed a higher number of fired action potentials than that in the sham surgery group, which was significantly suppressed by H-20 (300 μM) treatment (Fig. 3*A*). SNI-induced DRG nociceptive neurons had significantly lower rheobase, higher AP firing frequency, and RMP than sham surgery group neurons (Fig. 3 *B*–*D*). Notably, SNI-induced DRG nociceptive neurons pretreated with H-20 (300 μM) significantly increased the rheobase, down-regulated AP firing frequency, and RMP (Fig. 3 *B*–*D*). Thus, our data illustrated that SNI-induced hyperexcitability in nociceptive DRG neurons was significantly suppressed by H-20. Consistently, behavioral data revealed that i.t. H-20 at a dose of 30 nmol significantly reduced SNI-induced mechanical allodynia (onset of 30 min, duration of 90 min, Fig. 3*E*).

Chronic Intrathecal Injection of H-20 Doesn't Evoke Analgesic Tolerance. Accumulating evidence indicates that repeated opioid administration for chronic pain states evokes spinal microglial activation associated with analgesic tolerance (25–27). In the present study, naïve WT mice were intrathecally injected with H-20 (30 nmol)/morphine (2 nmol) daily for 7 d. Immunohistochemical results of the spinal cord showed that repeated i.t. morphine (2 nmol) administration induced significant microglial activation, which is in line with previous reports (26) (Fig. 4 *A* and *B*). Unlike morphine, repeated intrathecal H-20 (30 nmol) injection did not induce microglial activation in the spinal cord (Fig. 4 *A* and *B*). In addition, the expression of c-Fos in the spinal cord is a marker of nociceptive neuron activity and is more closely correlated with the analgesic effects of drugs (28). As shown in *SI Appendix*, Fig. 5 *A* and *B*, repeated morphine injection markedly increased the number of c-Fos–positive neurons in the spinal cord compared with the saline group. The number of c-Fos–positive neurons in the H-20 group was even lower than that in the saline group ($P < 0.05$), indicating that H-20 does not cause opioid-related hyperalgesia.

As shown in Fig. 4*C* and *SI Appendix*, Fig. 5*C*, morphine (20 nmol) was used as a positive control with equal analgesic effect to H-20 (30 nmol) in the CFA model to assess tolerability of the drug. Repeated i.t. injection of H-20 (30 nmol) for 7 consecutive days produced equivalent analgesic effects (Fig. 4*C* and *SI Appendix*, Fig. 5*D*), whereas in the morphine group, the antiallodynic effect was significantly decreased on test day 7 (Fig. 4*C*), which is consistent with previous studies showing that repeated spinal morphine injections evoked antinociceptive tolerance in mice (26). As the area under the curve (AUC) graph shows, compared with day 1, no significant differences were observed on day 7 in the H-20 treatment group (Fig. 4*D* and *SI Appendix*, Fig. 5*E*, male, $P = 0.19$; female, $P = 0.89$). Repeated morphine administration diminished antinociception, but this decrease did not reach statistical significance (Fig. 4*D*, $P = 0.07$). These results indicated that spinal chronic treatment with H-20 did not produce tolerance with potent analgesic efficacy.

Spinal H-20 Exhibits Less Abuse Liability. The addiction potentials of spinal H-20 were estimated using the conditioned place preference (CPP) test (*SI Appendix*, Fig. 5*F*). In the CPP test, i.t. administration of saline had no effect in an unbiased paradigm (7.3 ± 17.1 s). In line with the research by Wang et al. (26), i.t. morphine (2 nmol) produced a significant increase in the drug-treated chamber (Fig. 4*E*). In contrast, spinal H-20 (30 nmol) displayed a significantly reduced CPP response compared with the morphine group (Fig. 4*E*). According to the results gathered in the CPP assay, i.t. H-20 exhibited reduced abuse liability compared with morphine.

Spinal H-20 Doesn't Induce Depressive/Anxious-Like Behaviors. The comorbidity of depression and anxiety can aggravate pain severity and affect the efficacy of drug intervention. As part of our continuing studies, the forced swim test (FST) and open field test were used to evaluate the depressive/anxious effects of spinal H-20/morphine treatment (Fig. 4*F* and *SI Appendix*, Fig. 5 *G*–*L*). In the FST, the immobility time of saline, H-20 (30 nmol) and morphine (2 nmol) were 153.9 ± 16,

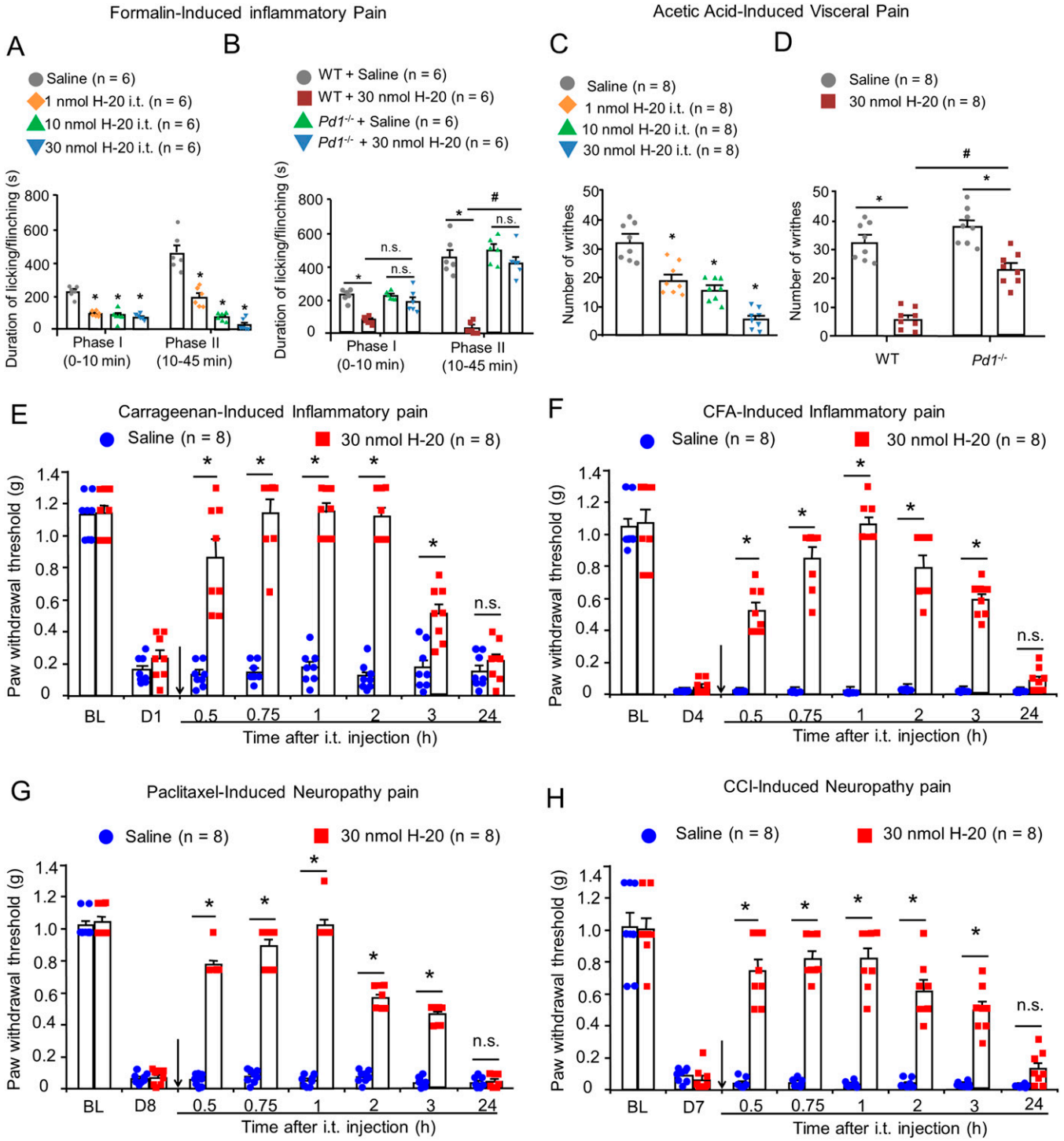

Fig. 2. Spinal H-20 produces potent analgesia via PD-1 in multiple preclinical pain models. (*A*) Antinociceptive effects of i.t. H-20 (1, 10, and 30 nmol) in formalin-induced inflammatory pain. Mean ± SEM 6 mice per group. *$P < 0.05$, versus saline group. Two-way RM ANOVA. (*B*) The effects of *Pd1* knockout on H-20 (30 nmol)-induced analgesia in formalin test. Mean ± SEM 6 mice per group. *$P < 0.05$, versus WT + saline group, $^{\#}P < 0.05$, versus WT + H-20 group. n.s., no significance. Three-way RM ANOVA. (*C*) Antinociceptive effects of i.t. H-20 (1, 10, and 30 nmol) on visceral pain model. Mean ± SEM 8 mice per group. *$P < 0.05$, versus saline group. One-way ANOVA. (*D*) The effects of *Pd1* knockout on H-20 (30 nmol)-induced analgesia in visceral pain test. Mean ± SEM 8 mice per group. *$P < 0.05$, versus saline group, $^{\#}P < 0.05$, versus WT + H-20 group. Two-way ANOVA. (*E–H*) Effects of spinal H-20 (30 nmol) on inflammatory factors, chemotherapeutics and nerve injury–induced mechanical allodynia. Mean ± SEM 8 male mice per group. *$P < 0.05$, versus saline group. n.s., no significance. Two-way RM ANOVA. (*E*) Carrageenan-induced acute inflammatory pain model. (*F*) CFA-induced chronic inflammatory pain model. (*G*) Paclitaxel-induced neuropathic pain model. (*H*) CCI-induced neuropathic pain.

140 ± 6.5, and 170 ± 7.8 s, respectively, and indicated that both H-20 (30 nmol) and morphine (2 nmol) do not exacerbate depression in the FST. Interestingly, spinal H-20 injection at a dose of 60 nmol significantly reduced the immobility time in the FST, which indicated that H-20 has an additional antidepressant effect at high dose (*SI Appendix*, Fig. 5*M*). Further investigations are required to understand the antidepressant mechanisms of H-20 in the future. In the open field test, the total time spent in the center area and the frequency of entry into the central zone were calculated as the parameter for

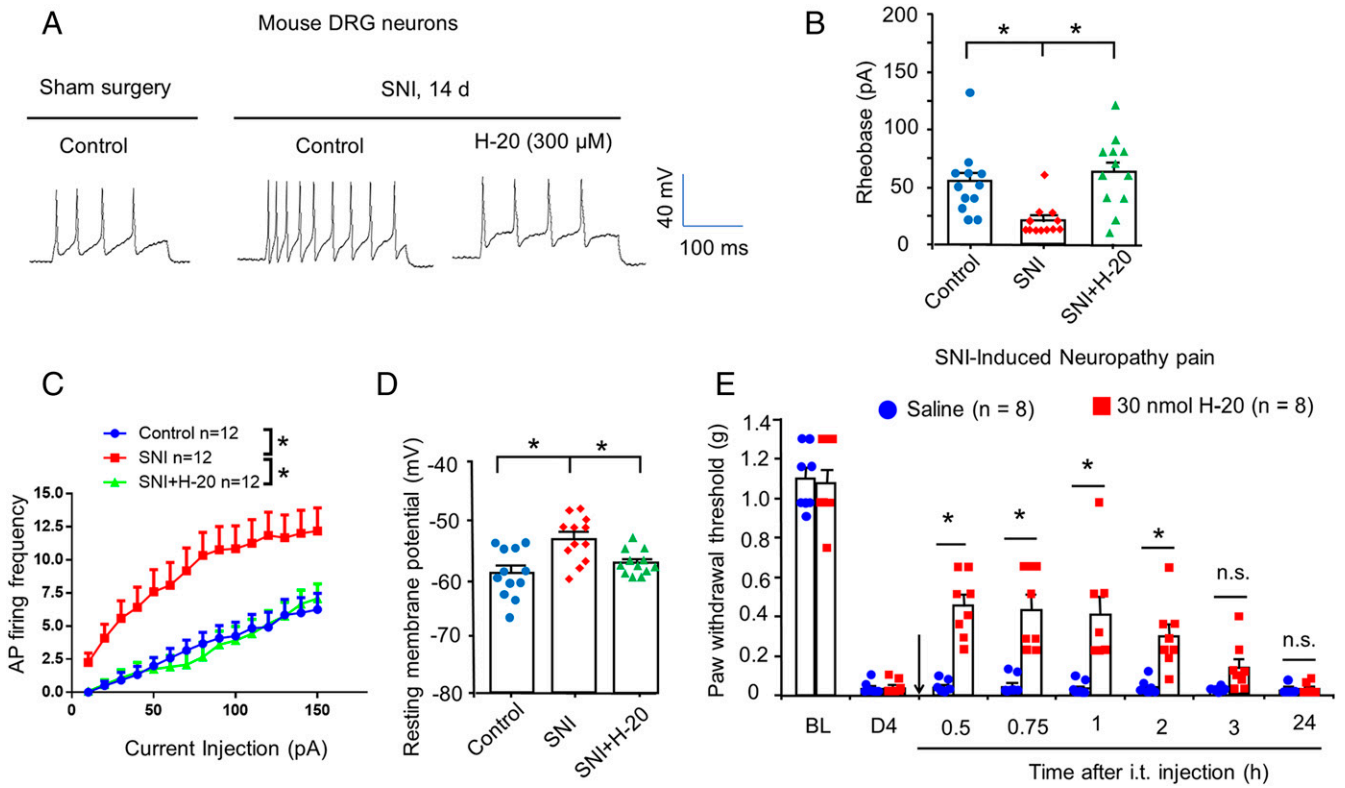

Fig. 3. H-20 inhibits neuronal hyperexcitability and neuropathic pain after nerve injury. (*A–D*) H-20 attenuated the SNI-induced mouse DRGs neuronal hyperexcitability. *$P < 0.05$, versus SNI group. Twelve neurons per group. (*A*) Traces of AP of SNI mice DRGs from 2 wk after surgery and the effects of H-20 (300 μM). (*B*) Rheobase. One-way ANOVA. (*C*) Frequency of AP. Two-way RM ANOVA. (*D*) RMP. One-way ANOVA. (*E*) Intrathecal H-20 (30 nmol) inhibits SNI-induced mechanical allodynia. Mean ± SEM 8 mice per group. *$P < 0.05$, versus saline group. n.s., no significance. Two-way RM ANOVA.

anxiety. No intergroup differences were observed (*SI Appendix*, Fig. 5 *I* and *J*).

H-20 Has Few Adverse Effects on Gastrointestinal Function. The ability of analgesic drugs to inhibit gastrointestinal function is also a nonnegligible side effect. As shown in Fig. 4 *G* and *H*, H-20 (30 nmol) had slightly negative effects on the gastrointestinal functions of mice, which were comparable to those of morphine (2 nmol). Treating mice with H-20 (1 or 10 nmol) did not affect the pellet number or dry weight (*SI Appendix*, Fig. 5*N*). After i.t. injection of H-20 (30 nmol) for 10 consecutive days, the same level of gastrointestinal function inhibition effects as those of the morphine-treated mice (2 nmol) was observed in the longer-term constipation test (*SI Appendix*, Fig. 5*O*).

Intrathecal H-20 Doesn't Affect Motor Function. The potential influence of spinal H-20 on the motor function of mice was estimated using the rotarod test. When compared with the saline-treated mice, both spinal H-20 (30 nmol) and morphine (2 nmol) did not change the length of time that the mice stayed on the rotarod (Fig. 4*I*, $P > 0.05$), suggesting that there was no motor impairment. This conclusion was further confirmed by the results of an additional open field test that no significant difference was noted in total distances (*SI Appendix*, Fig. 5*K*) and mean velocity (*SI Appendix*, Fig. 5*L*).

Intrathecal H-20 Induces Analgesia without Acute Itch. Itch is a common opioid-related adverse effect. In this study, spinal morphine (2 nmol) significantly evoked itch-related scratching behaviors in naïve WT mice in accordance with the findings of Wang et al. (29). On the contrary, the scratching response of H-20–treated mice was not different from that of the saline group (*SI Appendix*, Fig. 5*P*).

Discussion

To solve the opioid crisis, searching for alternative candidate compounds or analgesic targets is an important topic in the current study. Recently, researches have unveiled that PD-1 expressed on the DRG neurons is involved in the regulation of nociceptive signals (11, 12, 16). Although, it was proposed as an alternative therapeutic target in acute and chronic pain (15, 30), no small molecule drugs have yet been reported. The present study aimed to open an avenue for developing therapeutic analgesic peptides based on the PD-1 signaling pathway.

In this manuscript, promising PD-1 peptide ligand H-20 (Ile-Ser-Tyr-Gly-Gly-Ala-Asp-Tyr-Lys-OH) was screened via virtual screening. Furthermore, H-20 was synthesized via solid-phase synthesis and further evaluated for its analgesic properties at cellular, organizational, and behavioral levels. According to the in vitro results, H-20 significantly induced SHP-1 phosphorylation, attenuated the capsaicin-induced $[Ca^{2+}]_i$ increase, and modulated neuronal excitability via PD-1 with micromolar affinity. In addition, we found that i.t. administration of H-20 (30 nmol) could increase the basal pain threshold of WT mice. When *Pd1* is knocked out, the mechanical pain threshold of mice was decreased and no longer altered by H-20.

The multiple preclinical pain models, including those for formalin-/carrageenan-/CFA-induced inflammatory pain, acetic acid–induced visceral pain, and PTX-/CCI-/SNI-induced neuropathic pain, were used to investigate the analgesic potential of H-20 after i.t. administration. We found that spinal H-20 at the 30 nmol dose significantly alleviated acute inflammatory

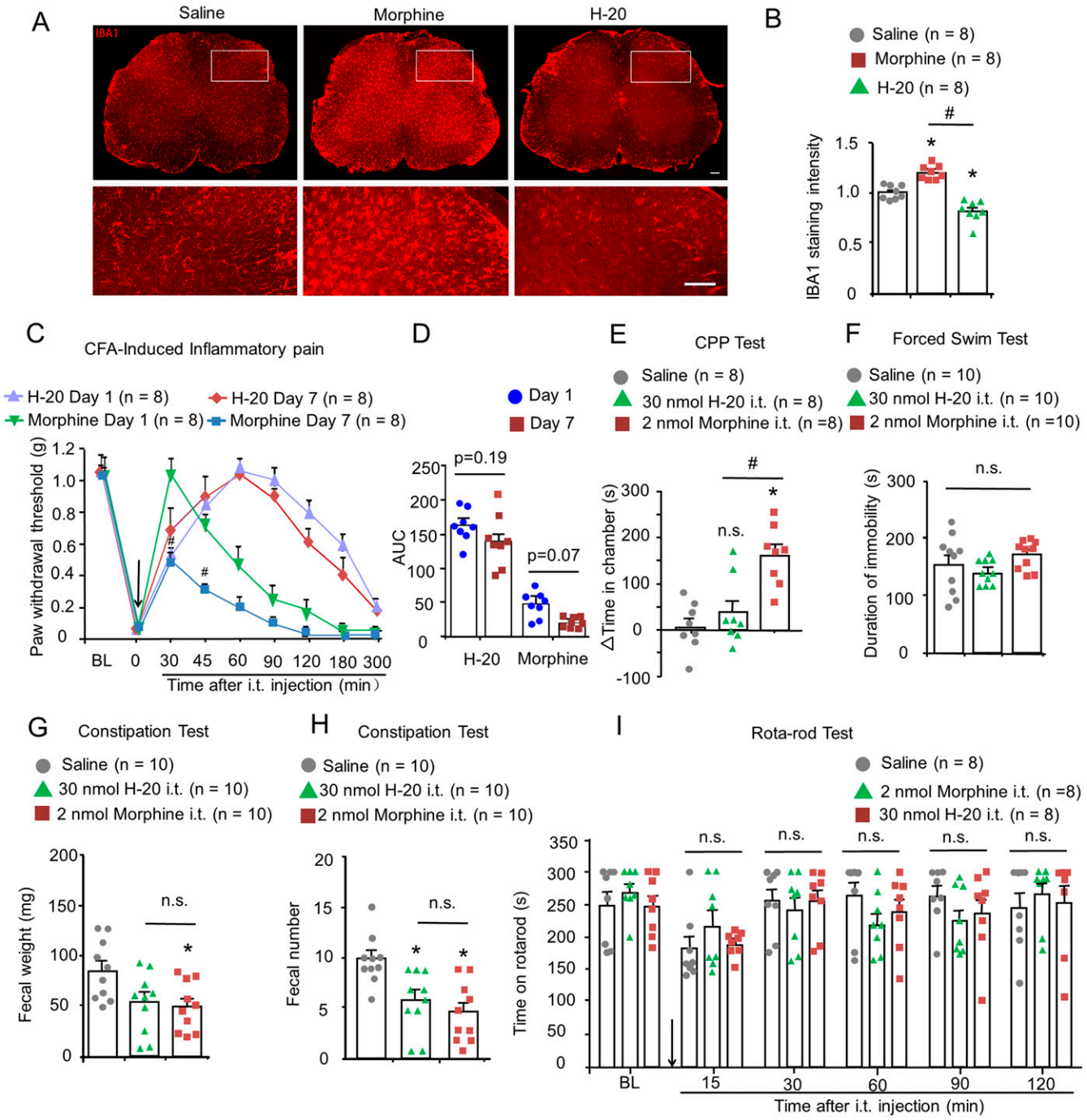

Fig. 4. Adverse effects evaluation of spinal H-20 in mice. (*A*) The expression of microglial in spinal cord after repeated i.t. H-20 (30 nmol)/morphine (2 nmol) for 7 continuous days. (Scale, 50 μm.) (*B*) Quantification of IBA1-integrated intensity. Mean ± SEM $^{*}P < 0.05$, versus saline group. $^{\#}P < 0.05$, versus morphine group. Four mice per group, eight images per group. One-way ANOVA. (*C*) Antinociception of i.t. repeated H-20 (30 nmol) or morphine (20 nmol) in CFA model. Mean ± SEM 8 mice per group. $^{\#}P < 0.05$, versus day 1. Three-way RM ANOVA. (*D*) The AUC values of H-20 and morphine on days 1 and 7. Two-way ANOVA. (*E*) Effect of repeated i.t. H-20 and morphine on CPP test. Mean ± SEM, 8 per group. $^{*}P < 0.05$, versus saline group. $^{\#}P < 0.05$, versus morphine group. n.s., no significance. One-way ANOVA. (*F*) Effect of i.t. H-20 and morphine on the immobility time in the forced swim test. Mean ± SEM, 10 mice per group, n.s., no significance. One-way ANOVA. (*G* and *H*) Effect of i.t. H-20 and morphine on gastrointestinal function. Mean ± SEM, 10 mice per group. $^{*}P < 0.05$, versus saline group. n.s., no significance. One-way ANOVA. (*I*) Effects of i.t. H-20 and morphine on motor coordination in mice. Mean ± SEM, 8 mice per group. n.s., no significance. Two-way RM ANOVA.

pain, visceral pain, and chronic inflammatory pain. Although H-20 had a half-life of 100 min, the analgesic effects of H-20 were sustained up to 3 to 5 h in pain models, which may be due to the complexity of in vivo drug metabolism of peptides, and warrant future studies. In addition, we did not observe spinal analgesic efficacy differences of H-20 between female and male mice in chronic inflammatory pain.

In the formalin test, the analgesic activity of H-20 was compared with that of PD-L1. Despite a more-than 100-fold analgesic efficacy lower than PD-L1, H-20 has more unique structural advantages and promising application prospects in the research and development of analgesic drugs. Furthermore, SHP-1 inhibitor SSG and $Pd1^{-/-}$ mice were used to further identify the targets of H-20 in vivo after i.t. coadministration

in formalin and visceral assays. It is clear from the results that knockdown of the *Pd1* gene or inhibition of PD-1 downstream SHP-1 signaling reversed the analgesic effect of H-20. H-20 inhibited pain by binding to PD-1 and activating SHP-1 signaling pathways in accordance with in vitro assays. In our results, we found that the spinal analgesic effects of H-20 partially were reversed by SSG in the antagonistic experiments, which might be due to the multiple downstream pathways of PD-1 involved in analgesia processes, including the phosphorylation of SHP-1 (10, 12). In addition, given the complexity of the pathogenesis of pathologic pain, the PD-1/SHP-1 pathway is not the only regulator of pain (31–33).

Patients suffering from neuropathic pain account for ∼7 to 10% of the general population (34). Neuropathic pain, defined as "pain caused by a lesion or disease of the somatosensory nervous system" (35), is more difficult to treat clinically without decent medical care in all pain paradigms. Many analgesics have marginal therapeutic efficacy to alleviate neuropathic pain (36). More meaningfully, spinal H-20 displayed potent and long-lasting antineuropathic effects in multiple chronic neuropathic pain models (CIPN, CCI, and SNI). The hyperexcitability of nociceptive neurons elicited by nerve injury has been confirmed to be associated with chronic neuropathic pain (37). In agreement with behavioral results, H-20 pretreatment significantly reduced the SNI-induced DRG neuron hyperexcitability from electrophysiological recordings.

Finally, analysis of the data obtained from the side-effect evaluation experiments showed that H-20 at analgesic doses had minimal unwanted side effects, analgesic tolerance, abuse potential, depression, anxiety, constipation, motor impairment, and itch. Furthermore, H-20 showed a slight but significant antidepressant effect. Thus, developing a new analgesic therapy using PD-1 signaling to therapeutically alleviate chronic pain is feasible and worthy of future research.

Materials and Methods

Reagents and Animals. H-20 (Fig. 1*A* and *SI Appendix*, Table 2) with a purity of 98% was synthesized by GL Biochem (Shanghai Ltd) using a solid-phase synthesis strategy. The molecular weight of H-20 is 973.04 g/mol. Fluo-4 AM (F14201) was purchased from Thermo Fisher Scientific. Morphine hydrochloride was obtained from the Shenyang First Pharmaceutical Factory and stored at −20 °C. SSG was purchased from Merck Millipore. Recombinant mouse PD-L1 protein (mPD-L1, Fc Chimera, ab216192) was obtained from Abcam. Mouse PD-1 protein (mPD-1, ECD, His Tag, cat. no. 50124-M08H) was purchased from Sino Biological. ICR mice were acquired from the Experimental Animal Center of Nantong University. *Pd1* gene knockout mice on a C57BL/6 background were obtained from the Innovation Center of Neuroregeneration of Nantong University. Mice were housed at 22 ± 2 °C, under a 12 h light/dark cycle. All behavioral assays were carried out between 9:00 AM and 5:00 PM. All experiments were approved by the Experimental Animal Protection and Care Committee of Nantong University (permission no. S20210226-036).

Binding Mode Prediction. The binding model of H-20 with PD-1 was predicted as previously described (38), and the crystal structure of PD-1 (PDB ID: 4ZQK) was downloaded from the Protein Data Bank. The critical residues in the PD-1 binding pocket were Val^{64}, Tyr^{68}, Gln^{75}, Thr^{76}, Lys^{78}, Asp^{85}, Ile^{126}, Leu^{128}, Ala^{132}, Ile^{134}, and Glu^{136}. The binding model was viewed and analyzed by using the Glide peptide docking software package (39). The binding scoring was obtained again using MM-GBSA.

MST Assay. The binding affinity of H-20/mPD-L1 to mPD-1 protein was measured using MST. The experimental procedures were performed as previously reported (20). Briefly, mPD-1 was prelabeled with Monolith NT Protein Labeling Kit Red and then incubated with H-20/mPD-L1 at 25 °C. The starting concentration of mPD-L1 and H-20 were 10 μM and 2 mM, respectively. After incubation for 5 min, the reaction solutions were detected using Monolith NT.115Pico (Nano Temper). The dissociation constant (K_D) was calculated using NT Analysis software (Nano Temper Technologies).

Metabolic Stability. The stability of H-20 was investigated by incubation with mouse brain homogenate as described previously (40). Briefly, 10 μL of H-20 (10^{-2} M) was incubated at 37 °C with the 190 μL of mouse brain homogenate (2.1 mg/mL). H-20 was used at a final concentration of 0.5 mM. The supernatants were monitored at various time points by reverse-phase high performance liquid chromatography (RP-HPLC). The degradation $t_{1/2}$ of H-20 was calculated as follows: $t_{1/2} = \ln 2/\kappa$. The degradation rate constant (κ) was calculated using linear regression.

Primary DRG Neuron Culture. Cultured DRG neurons separated from male C57BL/6 and $Pd1^{-/-}$ mice were used for calcium imaging and patch-clamp recordings. DRGs were harvested from mice under isoflurane anesthesia and incubated for 60 min at 37 °C in collagenase A (0.2 mg/mL, Roche). After incubation, DRG neurons were placed on poly-D-lysine–coated glass coverslips and nourished with neurobasal defined medium supplemented with 2% B_{27} supplement at 37 °C with 5% CO_2 overnight before the experiments.

Calcium Imaging. Cultured DRGs were loaded with the calcium indicator Fluo-4 AM at 37 °C for 30 min. Then, the cells were incubated with H-20 in Hanks' balanced salt solution (HBSS) (Gibco, with calcium, magnesium, and glucose, but no Phenol Red) for an additional 30 min. DRGs were depolarized with capsaicin (2 μM). The fluorescence intensity of free Ca^{2+} in cells was monitored using a confocal microscope (excitation 490 nm, emission 520 nm).

Immunofluorescence. After appropriate survival times, mice were anesthetized with isoflurane. Spinal cord (L4-L5)/DRG (L3–L5) segments were obtained after perfusion with phosphate-buffered saline (PBS) and 4% paraformaldehyde. The tissues were postfixed in 4% paraformaldehyde and cryoprotected in a 30% sucrose solution. The tissues were embedded inoptimal cutting temperature (OCT) compound medium in advance and sliced into transverse sections (spinal cord sections, 30 μm; DRG sections, 12 μm) with a microtome. After blocking in 3% BSA for 2 h, the sections were incubated overnight at 4 °C with the following primary antibodies: anti–PD-1 (1:500, Sigma, rabbit)/anti-HA (1:2,000, Sigma, rabbit)/anti–pSHP-1(1:500, Abcam, rabbit)/IBA 1 (1:1,000, NOVUS, goat). After washing with PBS, the sections were incubated with a Cy3-conjugated secondary antibody (1:1,000) overnight at 4 °C. Images were captured with a Nikon fluorescence microscope.

Patch-Clamp Electrophysiology. Patch-clamp recording tests were performed using an EPC10 amplifier (HEKA) and patch master software as described previously (11). Pipettes were pulled from borosilicate capillaries and polished to 4 to 6 MΩ resistance. Recordings were filtered at 2 kHz and sampled at 10 kHz. For AP and RMP recordings, the pipette solution contained the following (in millimoles): 126 K-gluconate, 10 ethylene glycol tetraacetic acid (EGTA), 10 NaCl, 1 $MgCl_2$, 2 NaATP, and 0.1 MgGTP, pH 7.3 (adjusted with KOH). The external solution contained the following (in millimoles): 140 NaCl, 5 KCl, 2 $CaCl_2$, 1 $MgCl_2$, Hepes 10, and 10 glucose, pH 7.4 (adjusted with NaOH).

Drug Administration. Intrathecal injection of drugs was conducted in awake mice as described previously (41). The position of the i.t. injection was between the L5 and L6 vertebral segments. A 30-G needle was used for i.t. administration of the drug in a volume of 10 μL.

Formalin-Induced Nociceptive Behavioral. Mice were adapted to the observation box for 15 min. Drugs were intrathecally injected 5 min before subcutaneous intraplantar administration of 20 μL 5% formalin into the right hind paw as previously described (11). The cumulative time of nociceptive behaviors (biting, licking, and shaking injected paw) during phase I (0 to 10 min) and phase II (10 to 45 min) were recorded.

Visceral Pain. The drug was intrathecally injected 5 min before intraperitoneal injection of 1% acetic acid solution (10 mL/kg) as previously described (40). The pain-related behaviors (abdominal writhing responses) were recorded within 20 min.

Carrageenan/CFA-Induced Inflammatory Pain. The carrageenan/CFA-induced inflammatory pain model was established as previously described (42). Mice were acclimatized to the test environment for 2 d (3 h/day) prior to the experiments. The basal mechanical threshold was measured before surgery by the von Frey test. Intraplantar injections of 20 μL 1% λ-carrageenan/CFA-induced mechanical allodynia. After intrathecal injection of H-20/saline, the mechanical sensitivity was measured at 0.5, 0.75, 1, 2, 3, and 24 h.

Neuropathic Pain. PTX-induced peripheral neuropathy, causing severe functional impairment, is one of the side effects of antineoplastic substances. The PTX-induced neuropathy model was produced as previously described by Dougherty and coworkers (43). Briefly, intermittent intraperitoneal injection of PTX (2 mg/kg) at 10:00 to 12:00 AM on days 1, 3, 5, and 7. The final cumulative dose of PTX was 8 mg/kg per mouse. The mechanical sensitivity of neuropathic pain in mice was tested using the von Frey method. After i.t. administration of H-20/saline, the paw withdrawal threshold was measured as described for the carrageenan/CFA model.

A CCI-induced neuropathic pain model was generated as previously described (26, 44). Mice were continuously anesthetized with isoflurane. For CCI mice, the left sciatic nerve of mice was tied loosely with 3 to 8.0 silk (interval, 1 mm). The SNI model was prepared according to the methods of Bourquin et al. (45). Mice were continuously anesthetized with isoflurane. For SNI mice, the muscle tissue was bluntly separated to expose the left sciatic nerve. The peroneal and tibial nerves were knotted with silk thread and transected at the lower end of the ligature with the sural nerve remaining intact. The wound was sutured and debrided with iodine. The mechanical sensitivity of the neuropathic pain mice was tested using the von Frey method. After i.t. administration of H-20/saline, the paw withdrawal threshold was measured as described for the carrageenan/CFA model.

Antinociceptive Tolerance. In the CFA model, repeated drug injections were performed for 7 consecutive days to estimate the development of tolerance to H-20 (30 nmol)/morphine (20 nmol). The analgesic efficacy was measured on days 1 and 7 as described above for the CFA model.

CPP Test. The CPP test was performed as described previously (26). Briefly, mice were acclimatized to the CPP apparatus (Thinker Tech Nanjing Biotech Limited Co., QAXK-CPP) for 15 min 1 d prior to the experiment (day 0). On test day 1, a mouse was randomly placed into a chamber and allowed free spontaneous activity in both chambers for 15 min. The mice with appropriate residence times on one chamber (360 s $\leq$t $\leq$ 540 s) were selected for the next step. On test days 2 to 4, the mouse was limited to one chamber in the morning for 15 min after intrathecal saline injection. Six hours later, the mouse was i.t. injected with saline/H-20/morphine and limited to the opposite chamber for 15 min. On test day 5, the time of the mice with free access to the entire apparatus was recorded for 15 min. Preference for the H-20/morphine-paired chamber was calculated.

FST. The potential risk of depressive effects evoked by H-20 was tested using the FST (46). Briefly, 30 min after i.t. injection of H-20 (30 nmol)/morphine (2 nmol)/saline, ICR mice (20 g) were forced to swim in water (20 ± 3 °C) and recorded for 6 min with a videocamera. The duration of immobility was calculated for the time period of 2 to 6 min.

Constipation Test. ICR mice (25 to 30 g) pretreated by fasting for 16 h were used to assess the inhibitory effects of H-20/morphine on gastrointestinal function as described previously (40). After intrathecal injection of the drug, the number and dry weights of the fecal pellets within 1 h were recorded.

Rotarod Test. A standard rotarod apparatus (RWD Life Science Co., Ltd, LE 8500) was used to evaluate the motor impairment of mice as described previously (11). Mice were pretrained for 2 consecutive days. On test day 3, after H-20 (30 nmol)/morphine (2 nmol) administration, the mice were placed on a rod. The rotational speed was gradually increased from 4 to 40 rpm with 10 min. The time spent on the accelerating rotarod was recorded at 15, 30, 60, 90, and 120 min.

Statistical Analysis. The data were analyzed by GraphPad Prism 6.0 and are provided as the means ± SEM. Statistical analyses were performed by analysis of variance (one-way, two-way, three-way, or repeated measures ANOVA) followed by post hoc Bonferroni's test or Student's *t* test. Statistical significance was accepted when $P < 0.05$. Densitometry analysis of the images was calculated and analyzed using ImageJ software.

Data Availability. All study data are included in the article and/or supporting information.

ACKNOWLEDGMENTS. We thank Professor Yi Shen for her guidance in the statistical analysis of data. We acknowledge support from the National Natural Science Foundation of China (82101302 and 32070998), the National Key Research and Development Program of China (2017YFA0104704), the Key Research and Development Program (Social Development) of Jiangsu Province (BE2020667), the Foundation of Jiangsu Province "333 Project High-Level Talents" (BRA2020076), Six Talent Peaks Project in Jiangsu Province (2017-SWYY-056), Jiangsu Province Innovation And Entrepreneurship Training Program for College Students (202110304030Z), the Nantong Civic Science and Technology Project of China (JC2021113), and Priority Academic Program Development of Jiangsu Higher Education Institutions.

Author affiliations: [a]Center for Basic Medical Research, Medical School of Nantong University, Nantong 226001, Jiangsu Province, China; [b]Department of Histology and Embryology, Medical School of Nantong University, Nantong 226001, Jiangsu Province, China; [c]Key Laboratory of Neuroregeneration of Jiangsu and the Ministry of Education, Co-Innovation Center of Neuroregeneration, Nantong University, Nantong 226001, Jiangsu Province, China; [d]Dr. Neher's Biophysics Laboratory for Innovative Drug Discovery, Macau Institute for Applied Research in Medicine and Health, State Key Laboratory of Quality Research in Chinese Medicine, Macau University of Science and Technology, Taipa, Macau, China; [e]Ministry of Education Key Laboratory of Functional Polymer Materials, State Key Laboratory of Medicinal Chemical Biology, Institute of Polymer Chemistry, College of Chemistry, Nankai University, Tianjin 300071, China; and [f]Department of Anesthesiology, Affiliated Hospital of Nantong University, Nantong 226001, Jiangsu Province, China

1. C. Stannard, Where now for opioids in chronic pain? *Drug Ther. Bull.* **56**, 118–122 (2018).
2. S. Mercadante, E. Arcuri, A. Santoni, Opioid-induced tolerance and hyperalgesia. *CNS Drugs* **33**, 943–955 (2019).
3. N. Volkow, H. Benveniste, A. T. McLellan, Use and misuse of opioids in chronic pain. *Annu. Rev. Med.* **69**, 451–465 (2018).
4. A. Henninot, J. C. Collins, J. M. Nuss, The current state of peptide drug discovery: Back to the future? *J. Med. Chem.* **61**, 1382–1414 (2018).
5. M. Muttenthaler, G. F. King, D. J. Adams, P. F. Alewood, Trends in peptide drug discovery. *Nat. Rev. Drug Discov.* **20**, 309–325 (2021).
6. I. W. Hamley, Small bioactive peptides for biomaterials design and therapeutics. *Chem. Rev.* **117**, 14015–14041 (2017).
7. A. Tyagi, E. B. Daliri, F. Kwami Ofosu, S. J. Yeon, D. H. Oh, Food-derived opioid peptides in human health: A review. *Int. J. Mol. Sci.* **21**, E8825 (2020).
8. S. Bagheri-Ziari, D. Shahbazzadeh, S. Sardari, J. M. Sabatier, K. Pooshang Bagheri, Discovery of a new analgesic peptide, leptucin, from the Iranian scorpion, *Hemiscorpius lepturus. Molecules* **26**, 2580 (2021).
9. Z. Dekan *et al.*, A tetrapeptide class of biased analgesics from an Australian fungus targets the μ-opioid receptor. *Proc. Natl. Acad. Sci. U.S.A.* **116**, 22353–22358 (2019).
10. J. Zhao, A. Roberts, Z. Wang, J. Savage, R. R. Ji, Emerging role of PD-1 in the central nervous system and brain diseases. *Neurosci. Bull.* **37**, 1188–1202 (2021).
11. G. Chen *et al.*, PD-L1 inhibits acute and chronic pain by suppressing nociceptive neuron activity via PD-1. *Nat. Neurosci.* **20**, 917–926 (2017).
12. C. Jiang *et al.*, PD-1 Regulates GABAergic Neurotransmission and GABA-Mediated Analgesia and Anesthesia. *iScience* **23**, 101570 (2020).
13. R. Makuku, N. Khalili, S. Razi, M. Keshavarz-Fathi, N. Rezaei, Current and future perspectives of PD-1/PDL-1 blockade in cancer immunotherapy. *J. Immunol. Res.* **2021**, 6661406 (2021).
14. S. Zhao, F. Li, R. K. Leak, J. Chen, X. Hu, Regulation of neuroinflammation through programed death-1/programed death ligand signaling in neurological disorders. *Front. Cell. Neurosci.* **8**, 271 (2014).
15. B. L. Liu, Q. L. Cao, X. Zhao, H. Z. Liu, Y. Q. Zhang, Inhibition of TRPV1 by SHP-1 in nociceptive primary sensory neurons is critical in PD-L1 analgesia. *JCI Insight* **5**, 137386 (2020).
16. Z. Wang *et al.*, Anti-PD-1 treatment impairs opioid antinociception in rodents and nonhuman primates. *Sci. Transl. Med.* **12**, eaaw6471 (2020).
17. C. J. Wienken, P. Baaske, U. Rothbauer, D. Braun, S. Duhr, Protein-binding assays in biological liquids using microscale thermophoresis. *Nat. Commun.* **1**, 100 (2010).
18. B. Gangadharan *et al.*, Molecular mechanisms and structural features of cardiomyopathy-causing troponin T mutants in the tropomyosin overlap region. *Proc. Natl. Acad. Sci. U.S.A.* **114**, 11115–11120 (2017).
19. N. Zeytuni *et al.*, Structural insight into the *Staphylococcus aureus* ATP-driven exporter of virulent peptide toxins. *Sci. Adv.* **6**, eabb8219 (2020).
20. W. Zhai *et al.*, Blocking of the PD-1/PD-L1 interaction by a novel cyclic peptide inhibitor for cancer immunotherapy. *Sci. China Life Sci.* **64**, 548–562 (2021).
21. Y. Yang *et al.*, Delayed activation of spinal microglia contributes to the maintenance of bone cancer pain in female Wistar rats via P2X7 receptor and IL-18. *J. Neurosci.* **35**, 7950–7963 (2015).

22. L. S. Premkumar, M. Abooj, TRP channels and analgesia. *Life Sci.* **92**, 415–424 (2013).
23. B. Melkes, V. Markova, L. Hejnova, J. Novotny, β-arrestin 2 and ERK1/2 are important mediators engaged in close cooperation between TRPV1 and μ-opioid receptors in the plasma membrane. *Int. J. Mol. Sci.* **21**, E4626 (2020).
24. A. K. Feehan, J. Morgenweck, X. Zhang, A. T. Amgott-Kwan, J. E. Zadina, Novel endomorphin analogs are more potent and longer-lasting analgesics in neuropathic, inflammatory, postoperative, and visceral pain relative to morphine. *J. Pain* **18**, 1526–1541 (2017).
25. H. Leduc-Pessah *et al.*, Site-specific regulation of P2X7 receptor function in microglia gates morphine analgesic tolerance. *J. Neurosci.* **37**, 10154–10172 (2017).
26. Z. Wang *et al.*, Spinal DN-9, a peptidic multifunctional opioid/neuropeptide FF agonist produced potent nontolerance forming analgesia with limited side effects. *J. Pain* **21**, 477–493 (2020).
27. J. Qu *et al.*, Blocking ATP-sensitive potassium channel alleviates morphine tolerance by inhibiting HSP70-TLR4-NLRP3-mediated neuroinflammation. *J. Neuroinflammation* **14**, 228 (2017).
28. A. Van Elstraete *et al.*, The opiorphin analog STR-324 decreases sensory hypersensitivity in a rat model of neuropathic pain. *Anesth. Analg.* **126**, 2102–2111 (2018).
29. Z. Wang *et al.*, Central opioid receptors mediate morphine-induced itch and chronic itch via disinhibition. *Brain* **144**, 665–681 (2021).
30. K. Wang *et al.*, PD-1 blockade inhibits osteoclast formation and murine bone cancer pain. *J. Clin. Invest.* **130**, 3603–3620 (2020).
31. G. Chen, Y. Q. Zhang, Y. J. Qadri, C. N. Serhan, R. R. Ji, Microglia in pain: Detrimental and protective roles in pathogenesis and resolution of pain. *Neuron* **100**, 1292–1311 (2018).
32. A. I. Basbaum, D. M. Bautista, G. Scherrer, D. Julius, Cellular and molecular mechanisms of pain. *Cell* **139**, 267–284 (2009).
33. Y. Huh, R. R. Ji, G. Chen, Neuroinflammation, bone marrow stem cells, and chronic pain. *Front. Immunol.* **8**, 1014 (2017).
34. O. van Hecke, S. K. Austin, R. A. Khan, B. H. Smith, N. Torrance, Neuropathic pain in the general population: A systematic review of epidemiological studies. *Pain* **155**, 654–662 (2014).
35. T. S. Jensen *et al.*, A new definition of neuropathic pain. *Pain* **152**, 2204–2205 (2011).
36. P. Basu, A. Basu, In vitro and in vivo effects of flavonoids on peripheral neuropathic pain. *Molecules* **25**, E1171 (2020).
37. J. M. Chung, K. Chung, Importance of hyperexcitability of DRG neurons in neuropathic pain. *Pain Pract.* **2**, 87–97 (2002).
38. Y. Wang *et al.*, PD-1-targeted discovery of peptide inhibitors by virtual screening, molecular dynamics simulation, and surface plasmon resonance. *Molecules* **24**, E3784 (2019).
39. Y. Wang *et al.*, Discovery of novel IDH1 inhibitor through comparative structure-based virtual screening. *Front. Pharmacol.* **11**, 579768 (2020).
40. L. Zhao *et al.*, Design, synthesis, and biological activity of new endomorphin analogs with multi-site modifications. *Bioorg. Med. Chem.* **28**, 115438 (2020).
41. J. K. Niehaus, B. Taylor-Blake, L. Loo, J. M. Simon, M. J. Zylka, Spinal macrophages resolve nociceptive hypersensitivity after peripheral injury. *Neuron* **109**, 1274–1282.e6 (2021).
42. B. Xu *et al.*, The multifunctional peptide DN-9 produced peripherally acting antinociception in inflammatory and neuropathic pain via μ- and κ-opioid receptors. *Br. J. Pharmacol.* **177**, 93–109 (2020).
43. Y. Li *et al.*, DRG voltage-gated sodium channel 1.7 is upregulated in paclitaxel-induced neuropathy in rats and in humans with neuropathic pain. *J. Neurosci.* **38**, 1124–1136 (2018).
44. C. Wetzel *et al.*, A stomatin-domain protein essential for touch sensation in the mouse. *Nature* **445**, 206–209 (2007).
45. A. F. Bourquin *et al.*, Assessment and analysis of mechanical allodynia-like behavior induced by spared nerve injury (SNI) in the mouse. *Pain* **122**, 14.e1–14.e14 (2006).
46. D. Zhao *et al.*, Structural features and potent antidepressant effects of total sterols and β-sitosterol extracted from *Sargassum horneri*. *Mar. Drugs* **14**, E123 (2016).